

”Study of an interaction between the jet and an  
interstellar medium of M87 with a spectral analysis by  
using *Chandra*”

S.Osone

Funabashi, Chiba, Japan, 273-0865.

e-mail : [osonesatoko@gmail.com](mailto:osonesatoko@gmail.com)

Abstract

Both a thermal component and a non thermal component as an interaction between the jet and an interstellar medium are studied with an exposure time of 800 ks of *Chandra*. It is confirmed that an X-ray energy spectra for the nucleus, the knot HST-1 and the knot D is well described with a power law as synchrotron emission. It is found that a power law model is rejected statistically for the knot A and an X-ray energy spectra is well described with a combination model of a power law and a thermal component. There is a possibility that gas in a jet is heated by a shock as interaction between the jet and an interstellar medium and it is observed as thermal emission. The flux of a non thermal bremsstrahlung from the jet as an interaction between accelerated electrons and an interstellar medium is calculated from an X-ray result with an effect of a break in an index and it is suggested that there is some contribution from the knot HST-1 to the observed flux with *Fermi*. This scenario matches with a non-flux variability in a GeV energy range.

Keywords:

Radio galaxy, gamma ray source, jet

1. Introduction

M87 is a close radio galaxy and is a center of the Virgo cluster. The distance is 16 Mpc ( $z=0.004$ ) (Tonry 1991). A mass of the black hole is estimated to be  $(3\sim 6)\times 10^9 M_{\odot}$  (Macchetto et al. 1997; Gebhardt & Thomas 2009).

M87 is observed over a wide spectrum from a radio frequency to TeV gamma ray. The TeV gamma ray emission from M87 were discovered by HEGRA (Aharonian et al. 2003)

and confirmed with HESS, VERITAS and MAGIC (Aharonian et al. 2006; Acciari et al. 2008; Albert et al. 2008). M87 has an inclined jet of 20 arc second length. The jet is resolved in a radio band with an angular resolution of 0.4 arc second, an optical band with an angular resolution of 0.7 arc second and an X-ray band with an angular resolution of 0.5 arc second of *Chandra*. The jet cannot be resolved in a high-energy range because *Fermi* has an angular resolution of 5.2 arc minutes and a Cherenkov image in TeV gamma ray has an angular resolution of 6 arc minutes. Therefore, the origin of TeV gamma ray is studied with both, a timescale of a flux variability and a correlation of flux with a simultaneous observation. A flux variability of a timescale  $t_{\text{val}}$  of 2 d in TeV gamma ray was observed (Aharonian et al. 2006). The size of the emitting area is given by  $ct_{\text{val}}\delta = 3.1 \times 10^{16} (\delta / 6)$  cm (0.01 pc). Here,  $c$  is a speed of a light and  $\delta$  is a Doppler factor. Therefore, they conclude that the origin of TeV gamma ray is the nucleus. A correlation between the nucleus with a radio of 43 GHz and TeV gamma ray with VERITAS also show the same result (Acciari et al. 2009). A correlation between X-rays of the nucleus and TeV gamma ray was detected in 2008 and 2010, while that between X-ray of the knot HST-1 and TeV gamma ray was detected in 2005 (Abramowaski et al. 2012). The knot HST-1 is also an origin of TeV gamma ray. Radio, optical, and X-ray observations of the nucleus are used for a study of multi wavelength energy spectra.

Non-simultaneous multi-wavelength energy spectra are described with various models (Reiger & Aharonian 2012). The models are classified into three categories: leptonic models, hadronic models and others. Leptonic models can be a homogeneous one-zone synchrotron self Compton model (Finke, Dermer and Bottcher 2008), a decelerating jet model (Georganopoulos, Perlman and Kazanas 2005), an electron of a jet model (Stawarz et al. 2005, 2006), a multi-blob model (Lenain et al. 2008), a spine-sheath layer model (Tavecchio & Ghisellini 2008), a jet in a jet model (Giannios, Uzdensky and Begelman 2010) and an external inverse Compton model (Cui et al. 2012). Hadronic models can be a proton synchrotron model (Reimer, Protheroe and Donea 2004), an interaction model between protons and an interstellar medium (Pfrommer & Enßlin 2003), and an interaction between protons and a cloud injected to the jet (Barkov, Ramon and Aharonian 2012). Others include a lepto-hadronic model (Reynoso, Medina and Romero 2011), a dark matter annihilation model (Baltz et al. 2000; Saxena et al. 2011) and a magnetospheric model (Levinson & Rieger 2011; Broderick & Tchekhovskoy 2015).

Recently, a detection of a diffused thermal component of 1 keV for a radio lobe of radio galaxies, Cen A (Stawarz et al. 2013; O'sullivan et al. 2013) and Fornax A (Seta, Tashiro and Inoue 2013) was reported.

There is a possibility of a thermal component for not only the radio lobe of a jet, but also

a jet itself. NANTEN found a monocular cloud along an X-ray jet for SS433 (Yamamoto et al. 2008). A closest cloud N4 is 20 pc from SS433. A CO density for N1 is  $3 \text{ cm}^{-3}$ . They insisted that the jet compresses an interstellar medium and monocular clouds were formed. There is a possibility that gas in a jet is heated by a shock and it is observed as thermal emission. For the north part of SS433, which matches with the monocular cloud N4, an X-ray energy spectra are well described with either a power law model or a thermal bremsstrahlung model of 6 keV (Moldowan et al. 2005). For the south part of SS433, which does not match with any monocular clouds, an X-ray energy spectra are well described with a combination model of a power law and a Mekal with 0.20 keV (Brinkmann et al. 2007) .

Dainotti et al. (2012) studied an interaction between high energy cosmic rays and an interstellar medium about the M87 jet with a morphological analysis of *Chandra* and pointed out the decreasing soft X-ray emission in a surrounding from the knot E to the knot F of the M87 jet as a cosmic ray cocoon. There is a possibility that soft X-ray is absorbed in the compressed interstellar medium.

The X-ray energy spectra of the M87 jet has been analyzed with *Chandra* (Wilson & Yang 2002; Marshall et al. 2002; Perlman & Wilson 2005; Sun et al. 2018). They fitted energy spectra with a power law model and obtained an acceptable fit.

Hot gas of the Virgo cluster centered at M87 has been reported with *XMM* (Belsole et al. 2001). The background for the jet is the sum of Cosmic X-ray background and Non X-ray background and hot gas of Virgo cluster. The emission of hot gas of Virgo cluster depends on a distance from the center. Therefore, background should be taken according to a distance from the nucleus. Perlman & Wilson (2005) and Sun et al.(2018) takes two neighboring regions, a south and a north of the whole jet as a common background for all part of the jet. This is not correct.

Both Wilson & Yang (2002) and Perlman & Wilson (2005) use only obsID 1808 with an exposure time of 13 ks for CCD. Marshall et al. (2002) use data with an exposure time of 38 ks for High Energy Transmission Grating Spectrometer. Its effective area is about one tenth of that of CCD and this statistics corresponds to 4 ks with CCD. There are two problems with poor statistics. Any models tends to be acceptable with poor statistics. The other is contamination of hot gas with poor statistics. There is some contamination of hot gas of the cluster shown as a line feature on the energy spectra which subtract background for obsID 1808. The subtraction of background is not enough with an exposure time of 13 ks. With more statistics, this contamination is expected to be less. This is the reason why high statistics by using all archive is needed.

In this thesis, statistics is improved largely with an exposure time of about 800 ks and

a correct subtraction of background is done with *Chandra*. Statistics is almost same with that of Sun et al.(2018).

Both a thermal component and a non thermal component as an interaction between the jet and an interstellar medium of M87 with a spectral analysis using *Chandra* are studied. An additional thermal component to a synchrotron emission from the M87 jet as heated gas by a shock is examined. The flux of non thermal bremsstrahlung as an interaction between accelerated electrons and an interstellar medium is calculated from an X-ray result and is compared with the observed flux with *Fermi*.

## 2.Observation with *Chandra*

The detector is CCD with frame time of 0.4 sec. All archive opened by 2018.6 is used.The target is the nucleus, the knot HST-1, the knot D and the knot A. These targets are saturated in a frame time of 3.2 sec. Data observed from 2000 Jul. to 2014 Dec. is called as a former data set and data observed from 2015 Mar. to 2018 Apr. is called as a latter data set.

## 3.Spectral analysis with *Chandra*

CIAO4.7 and CALDB 4.6.8 are used for a former data set. CIAO4.9 and CALDB 4.7.6 are used for a latter data set.

### 3.1 Image

The pixel size of CCD is 0.5 arc second and the half energy radius is 0.5 arc second. The image is smoothed with a Gaussian of 1 sigma = 0.5 arc second. The image of obsID 1808 with a ds9 tool is shown in figure 1. From left, the nucleus, the knot HST-1, the knot D, the knot A, and each background region are shown.

In order to exclude hot gas of the cluster, two neighboring regions, south and north of a same size and same distance from the nucleus, are taken as a background region for each part of the jet.

Positions of the extracted region for obsID 1808 are shown in table 1. Positions of bright spots are changed from data to data. Positions of the extracted region are decided by the image made with a ds9 tool for each datasets. The nucleus and the knot HST-1 cannot be sometimes resolved and are treated as the large nucleus. A radius of the extracted region is same with that of obsID 1808 for each part of the jet.

### 3.2 Data selection

CCD pixels for the nucleus and the knot HST-1 are sometimes piled up heavily because

of a high count rate. This heavy pile up distorts energy spectra around 2 keV and above 5 keV, and show a hard energy spectra. The count rate with no pile up is below 0.03 c/s and no data for all knots apply for no pile up. Therefore, data set with an observed count rate below 0.31 c/s is selected for each knot. The observed count rate of 0.31 c/s is estimated as a 5 % piled up contamination using a PIMMS tool. The model of an absorbed power law with a photon index 2.0 in frame time of 0.4 sec is used for the calculation. The large nucleus contains the nucleus and the knot HST-1, and has a large radius. Therefore, data set with an observed count rate below 0.62 c/s is selected for the large nucleus. The observation logs used are shown in table2a, 2b, 2c, 2d for a large nucleus, the nucleus, the knot HST, the knot D and the knot A, respectively. For the knot D and the knot A, all archive data sets are used and total exposure time is about 80 times as long as that of obsID 1808.

### 3.3 Energy spectra

Energy spectra are summed for a selected region and a background region, respectively. Data points are binned so that the minimum counts per bin are above 15. An effective area is made with no weight of a count rate and with a correction of a PSF which are suitable conditions for an analysis of a point source. An effective area (arf) and an energy response (rmf) are made for a selected region and a background region, respectively, for each datasets. A rmf may change during an observation time of 18 years. Therefore, an arf and a rmf are multiplied as a rsp for each datasets. A rsp for the summed energy spectra is calculated with a weight of an exposure time for a selected region and a background region, respectively.

The summed energy spectra which subtract background for a former data set and a latter data set is described with no line features and a contamination of hot gas of cluster is excluded successfully.

#### 3.3.1 Model fitting

CCD has a sensitivity from 0.2 keV to 10 keV. There is a quantum efficiency degradation by a contamination of an optical filter. An energy range above 0.3 keV, and especially above 0.5 keV is well calibrated. A lower limit of an energy for an energy spectra fitting is set as 0.5 keV.

The XSPEC tool is used for a model fitting. A thermal component as an interaction between the jet and an interstellar medium is studied. First, a power law model is used. When a power law model is rejected statistically, a combination model of a power law and an APEC is used. An APEC model is thermal bremsstrahlung with a metal. The

absorption in soft X-ray is caused by a photo electric effect of a neutral material in line of a sight from us to M87. A column density by a 21 cm radio observation is  $1.6 \times 10^{20} \text{ cm}^{-2}$  (Kalberia et al. 2005). This is due to our galaxy. An absorption in soft X-ray cannot be below a 21 cm radio observation value. At first, a photo absorption is set free. When a column density is below a 21 cm radio observation value, a photo absorption is fixed to a 21 cm radio observation value and the energy spectra is fitted.

### 3.3.2. Fitting result of a former data set

Result for both a former data set and a latter data set is shown respectively. The fitting results of energy spectra with an absorbed power law model for former data set is shown in table 3. Energy spectra are well described with an absorbed power law for the nucleus, the knot HST-1 and the knot D. For a large nucleus, the nucleus and knot HST-1, column densities are above a 21 cm radio observation value. For the knot D, a column density agrees with a 21 cm radio observation value within a 90 % confidence statistical error. For the knot A, a column density is quite low against a 21cm radio observation value. A low column density implies an existence of a soft excess. Therefore, a column density for the knot A is fixed to 21 cm radio observation value. When energy spectra for the knot A are fitted with an absorbed power law model,  $\chi^2 461.19$  with d.o.f =316 is obtained, which probability is  $1.72 \times 10^{-7}$  as shown in table 4. The deviation from an absorbed power law model is a 5.2 sigma significance. A model of an absorbed power law is rejected statistically. When a APEC model is added to a power law model,  $\chi^2 322.44$  with d.o.f =313 is obtained, which probability is 0.345 as shown in table 4. An absorbed combination model of a power law and an APEC is acceptable. A flux ratio of a thermal component to total is 8%. A temperature of an APEC model is 0.23 keV. The temperature is almost same with a thermal component from a jet for SS433 of 0.20 keV (Brinkmann et al. 2007), for For A of 1 keV (Seta, Tashiro and Inoue 2013) and for Cen A of 0.5 keV (Stawarz et al. 2013).

There is a soft X-ray absorption in the north surroundings from the knot E to the knot F (Dainotti et al. 2012). In the image without a smooth, this area is spread in the north surroundings from the knot E to the knot A. There may be a soft X-ray absorption in the north surroundings of the knot A. In this analysis, two neighboring regions, north and south, are taken as background. If there is a soft X-ray absorption in background, a soft excess will be shown in the energy spectra subtracted background. Therefore, a test is done for the knot A. Only south region is taken as a background and the energy spectra subtracted background is made. When an energy spectra is fitted with an absorbed power law, column density is quite low against a 21cm radio observation value. When column

density is fixed to a 21 cm observation value and the energy spectra is fitted,  $\chi^2$  475.64 with d.o.f =316 is obtained, which probability is  $1.50 \times 10^{-8}$ . The deviation from an absorbed power law model is 5.6 sigma significance. When a APEC model is added to a power law,  $\chi^2$  321.04 with d.o.f =313 is obtained, which probability is 0.365. All fitting parameters with three models are consistent with those of the analysis for two neighboring regions. It is confirmed that there is no possible effect of background on the energy spectra for the knot A.

### 3.3.3 Fitting result of a latter data set

The fitting result of an energy spectra with an absorbed power law for a latter data set is shown in table 5. For the nucleus, the knot HST-1, the knot D, an absorbed power model is statistically accepted. For the nucleus and the knot D, column densities are above a 21 cm radio observation value. For the knot HST-1, a column density agrees with a 21 cm radio observation value within a 90 % confidence statistical error. For the knot A, a column density is quite low against a 21cm radio observation value. However, a reasonable fit is obtained as shown in table 6 when a column density is fixed to a 21 cm radio observation value. The probability of a deviation from an absorbed power law is 0.00928 (2.6 sigma). The reason why thermal emission is not needed for a latter data set may be statistics. Because 1 keV flux of a latter data set is low compared with that of a former data set, any model tends to be accepted statistically.

For the large nucleus, there is an excess above 7 keV. The probability of a deviation from an absorbed power law model is 0.0030 (3.0 sigma ) for the nucleus and  $4.5 \times 10^{-10}$  for the large nucleus. For the nucleus, an absorbed power law model is not rejected statistically. There is a hard X-ray detection from the nucleus with NuSTAR at 2017.2(Wong et al. 2017) and there is a corresponding data of both the nucleus and a large nucleus with *Chandra* in a latter data set. The excess above 7 keV for a large nucleus may be related with a hard X-ray detection. There is also a hard X-ray detection from the knot HST-1 with Suzaku at 2006.11(Jong et al. 2015). There is no corresponding data in a former data set of the knot HST-1 with *Chandra* because of a pile up.

### 3.3.4 Fitting result for all data

A former data set and a latter data set are summed. The fitting result of energy spectra with an absorbed power law model for all data is shown in table 7. For the nucleus, the knot D, an absorbed power law model is statistically accepted. For these targets, column densities are above a 21 cm radio observation value. For the knot HST-1, a column density is quite low against a 21cm radio observation value. However, a reasonable fit is

obtained as shown in table 8 when a column density is fixed to a 21 cm radio observation value.

When energy spectra is fitted with an absorbed power law for the knot A, a column density is quite low against a 21cm radio observation value. An absorbed power law model is rejected with a chance probability of  $7.9 \times 10^{-22}$  as shown in table 8 when a column density is fixed to 21cm radio observation value. The energy spectra is shown in figure 2(top). When an absorbed APEC model is added, a high temperature of 7 keV and high photon index of 3 is obtained as shown in table 8. A temperature of APEC model is obtained as 0.2 keV in a former data set. When temperature is fixed to 0.2 keV, a reasonable fit is obtained as shown in table 8. The energy spectra is shown in figure 2(bottom). This problem is under study. It is concluded definitely that an additional component is needed for the knot A.

When an energy spectra is fitted with an absorbed power law for a large nucleus, there is an excess above 7 keV as shown in figure 3. The probability of a deviation from an absorbed power law model is 0.0014(3.2 sigma) for the nucleus and  $2.7 \times 10^{-10}$  for a large nucleus. This is a tendency of a latter data set for both the nucleus and a large nucleus. For the nucleus, an absorbed power law model is not rejected statistically.

### 3.3.5 Comparison with *XMM* result

Bohringer et al. (2001) analyzed the X-ray energy spectra of an outer part of the jet with *XMM*. This location is 11 arc second apart from the nucleus, which is probably the knot A. The energy spectra of the jet is well described with an absorbed power law for both PN CCD and MOS CCD of *XMM*. Here, a column density is fixed to a 21 cm radio observation value.

There are two problems in their analysis. One is background and the other is signal to noise ratio. The location of a background is 20.8 arc second in north and 17.7 arc second in south for PN CCD, 22 arc second for MOS CCD from the nucleus. The distance is far from the source region. This is not correct. The exposure time is about 30 ks for both PN CCD and MOS CCD of *XMM* as compared with about 800 ks of *Chandra*. The effective area of PN CCD and MOS CCD of *XMM* are 1400 cm<sup>2</sup> and 800 cm<sup>2</sup> as compared with 300 cm<sup>2</sup> of CCD of *Chandra*. A FWHM of angular resolution of *XMM* is poor as 4 arc second and the radius of an extracted region is 4 arc second. The radius of a bright spot as the knot A is 1 arc second with *Chandra*. Therefore, the signal to noise ratio of PN CCD and MOS CCD of *XMM* is 1/10 and 1/14 of that of *Chandra* respectively. It is not strange that thermal component is not needed for an observation result with *XMM*.

## 4. Discussion

### 4.1 Physical values

For a former data set, a latter data set and all data, three physical values are calculated respectively: a neutral density  $N$  from a column density  $N_{\text{H}}$ , a density of accelerated electrons  $K'$  from both 1 keV flux and photon index of a power law and a plasma density  $n_{\text{H}} n_{\text{e}}$  from a normalization of an APEC model. Three physical values are shown in table 9.

#### 4.1.1 Neutral density

A column density by a 21 cm radio observation is due to our galaxy. The difference between a column density of 21cm radio observation and that from X-ray spectra analysis is considered as a cold medium around the M87 jet. A neutral density around the jet can be calculated with a size of an emission region. A neutral density  $N$  ( $\text{cm}^{-3}$ ) around each knot is calculated by dividing the difference of column densities with  $2R$ . Here,  $R$  is a emission radius for each knot.

#### 4.1.2 Density of an accelerated electron

Synchrotron emissivity  $J$  are given by  $2.344 \times 10^{-25} \times a(p) B^{(p+1)/2} K' (3.217 \times 10^{17} / \nu)^{(p-1)/2}$   $\text{W m}^{-3} \text{Hz}^{-1}$  (Longair 1992). Here, a density of an accelerated electron is given by  $dN_e/dE = K' E^{-p} \text{m}^{-3} \text{GeV}^{-1}$ .  $E$  is in units of GeV and  $K'$  is in units of  $\text{m}^{-3} \text{GeV}^{p-1}$ .  $B$  is a magnetic field in units of T. Various values of a magnetic field are reported from different analyses. An observation of a synchrotron self-absorption of the nucleus at 43 GHz sets a limit on a magnetic field from 1 G to 10 G (Kino et al., 2014). A timescale of an energy loss of synchrotron emission is proportional to  $1/B^2$  (Longair 1992). Harris et al. (2009) use the intensity which is integrated count rates from 0.2 keV to 17 keV for a pile up problem and discuss variability of an X-ray intensity with a short exposure of 5 ks. There is a contamination of hot gas of the cluster in an X-ray intensity. This is considered to be no problem because hot gas of the cluster is non variable with an energy resolution of CCD. Variability in X-ray is different for a different part of the jet. The nucleus is variable on a short timescale, the knot HST-1 and the knot D show a similar variability and the knot A is non variable over 10 years (Harris et al. 2009). This suggests a high magnetic field for the nucleus and a low magnetic field for other knots. An X-ray energy loss in the knot HST-1 is consistent with an  $E^2$  energy loss of synchrotron emission and a magnetic field of 0.6 mG for  $\delta=5$  is obtained (Harris et al. 2009). A magnetic field of 1 G is used for the nucleus and 1 mG is used for other knots. An index  $p$  is given by  $2\alpha - 1$  ( $\alpha$  is the photon index). A numerical parameter  $a(p)$  is a constant that depends on an

index  $p$ .  $a(3.0)$  is 0.269,  $a(3.5)$  is 0.217 and  $a(4)$  is 0.186 (Longair 1992).  $\nu$  is a frequency in units of Hz. A 1 keV flux of synchrotron emission is given by  $J V \Gamma^2 / 4\pi D^2$ . Here,  $V$  is a volume of the extracted region in units of  $\text{cm}^3$  which is given as  $4\pi R^3/3$ .  $R$  is a radius of the extracted region in units of cm as shown in table 1. Here,  $D$  is the distance of M87. Here,  $\Gamma$  is a Lorentz factor. There is a beaming effect for accelerated electrons. A solid angle in an observer system is  $1/\Gamma^2$  times as large as that in a jet system. An apparent velocity observed with the *Hubble Space Telescope* is different for each part of the jet and that for the knot HST-1 is  $6c$  that means an inclination angle of  $\theta = 19^\circ$  and a Lorentz factor of  $\Gamma = 3$  (Biretta, Sparks and Macchetto 1999; Meyer et al. 2013).  $K'$  is derived with a Lorentz factor  $\Gamma = 3$  for all parts of the jet.  $K'$  is small for the nucleus and large for other knots. This is due to a difference in a magnetic field against almost same X-ray flux.

#### 4.1.3 Plasma density

A normalization of an APEC is given as  $10^{-14} \times n_e n_i V / 4\pi D_A^2 (1+z)^2$ . Here,  $n_e$  is an electron density in units of  $\text{cm}^{-3}$  and  $n_i$  is an ion density in units of  $\text{cm}^{-3}$ .  $V$  is a volume of the extracted region in units of  $\text{cm}^3$ .  $D_A$  is an angular diameter distance to M87 in units of cm.  $z$  is a redshift. An electron density  $n_e$  is assumed to be equal to an ion density  $n_i$  and an ion density  $n_i$  is derived.

NANTEN observation of CO along an X-ray jet of SS433 suggests that a jet compresses an interstellar medium (Yamamoto et al. 2008). Dainotti et al. (2012) pointed out the decreasing soft X-ray emission in the surroundings from the knot E to the knot F as a cosmic ray cocoon. It is considered that a soft X-ray is absorbed in the compressed interstellar medium of the surroundings. The detection of a thermal component for the knot A is possible with this argument. The ratio of a temperature is given by  $T_2/T_1 = 2 \gamma (\gamma - 1) M^2 / (\gamma + 1)^2$  for strong shock  $M \gg 1$  (Longair 1992). Here,  $T_1$  is a temperature outside the jet and  $T_2$  is that in the jet.  $M$  is a mach number of a shock wave.  $\gamma$  is a ratio of a specific heat. When  $\gamma$  is given as  $5/3$  for monatomic gas,  $T_2/T_1 = 0.3 M^2 \gg 1$ . There is a possibility that the gas in the jet is heated by a shock and it is observed as thermal emission. The abundance of a thermal component is low compared with an intercluster medium of M87 which abundance is 1 solar (Belsole et al 2001). This suggests that the heating by a shock is occurred in the jet, not outside the jet. As supernova remnants, thermal gas and accelerated particles exist in the shock as different species and in different locations. The ratio of pressure is given by  $p_2/p_1 = 2 \gamma M^2 / (\gamma + 1)$  for a strong shock  $M \gg 1$  (Longair 1992). Here,  $p_1$  is pressure outside the jet and  $p_2$  is pressure in the jet. When  $\gamma$  is given as  $5/3$  for monatomic gas,  $p_2/p_1 = 1.25 M^2 \gg 1$ .

There is no pressure balance between the jet and an interstellar medium. The ratio of a density is given by  $\rho_2/\rho_1 = (\gamma + 1)/(\gamma - 1)$  for a strong shock  $M \gg 1$  (Longair 1992). Here,  $\rho_1$  is a material density outside the jet and  $\rho_2$  is that in the jet. When  $\gamma$  is given as 5/3 for monatomic gas,  $\rho_2/\rho_1 = 4$ . It is possible that a plasma density is comparable with a neutral density of a few  $\text{cm}^{-3}$ . The absorption in a cold medium and a soft excess are related. The observed normalization of a thermal component is a lower limit if there is a cold medium around the knot A.

The rotation measure for the knot A is  $\text{RM} \sim 200 \text{ rad m}^{-2}$  (Algaba, Asada, and Nakamura 2016). RM is given as  $8.12 \times 10^3 n_e B L$  (Longair 1992). Here,  $n_e$  is a plasma density in units of  $\text{m}^{-3}$ ,  $B$  is a magnetic field in units of T and  $L$  is a size of a region in units of pc. A plasma density is given as  $1.6 \times 10^{-3} \text{ cm}^{-3}$  with a magnetic field of 1 mG and a size of 156 pc for the knot A. This value differs from X-ray energy spectra by an order of 4. The lower limit of 90% confidence level statistical error of plasma density from X-ray energy spectra of former data set is  $8.7 \text{ cm}^{-3}$ . This difference needs more study.

#### 4.2. Non thermal bremsstrahlung

It is considered that there is an interaction between accelerated particles (proton, electron) and an interstellar medium. There may be the interaction between accelerated protons and an interstellar medium. Gamma ray from a pion decay can be detected from a shape of energy spectra which peak at 70 MeV. However, energy spectra below 100 MeV for M87 has not been published with *Fermi*. A high density of accelerated electrons from the jet is obtained. The flux of non thermal bremsstrahlung as an interaction between accelerated electrons and an interstellar medium is calculated.

##### 4.2.1 Calculated flux with *Chandra*

Flux of non-thermal bremsstrahlung for a cold material I is given as  $b N \int K \epsilon^{-p} / (p - 1) \text{ ph/m}^3/\text{s}/\text{J}$  (Longair 1992). Here,  $b$  is  $1.03 \times 10^{-21} \text{ m}^3/\text{s}$ .  $N$  is a neutral density in unit of  $\text{m}^{-3}$ .  $\epsilon$  is an energy in units of MeV. A number density of accelerated electrons is given as  $dN_e/dE = K(E)^{-p}$ .  $K$  is in units of  $\text{m}^{-3} \text{ J}^{p-1}$ .  $E$  is in units of J. A relation between  $K$  and  $K'$  is given as  $K' = (1.6 \times 10^{-10})^{p-1} K$ . A total energy loss rate  $dE/dt$  of a non-thermal bremsstrahlung for fully ionized materials differs from that for cold materials by a factor of 2 for  $100 < \gamma < 10^5$  (Longair 1992). Therefore, the same formula is used for fully ionized materials. Flux is given by  $I = V \Gamma^2 / 4 \pi D^2$ . Calculated flux of non-thermal bremsstrahlung is independent of  $\Gamma$  because  $\Gamma$  is used when  $K'$  is calculated from 1 keV flux of a power law. The calculated flux of non-thermal bremsstrahlung from an X-ray result is shown in table 10. The calculated flux is largely dependent on an index  $p$ . The

calculated flux of both a former data set and a latter data set of the knot HST-1 and a former data set of the knot A is high.

There is a peak in the energy spectra of  $E^2 dN/dE$  vs.  $E$  from a radio to an X-ray, where is a ultra violet. This break is not due to a synchrotron self absorption which is shown in a radio band. When this energy spectra is assumed as synchrotron emission, the derived spectral index of an electron distribution  $dN/dE$  has a break in the energy range from several hundred GeV to TeV and an index of an electron distribution  $dN/dE$  is about 2 in a low energy and about 4 in a high energy (Sun et al. 2018). The synchrotron emission from electrons which have an energy  $E$  peaks at an energy of  $(E/m_e c^2)^2 (eB/2\pi m_e)$  (Longair 1992). Here,  $B$  is a magnetic field. 1 keV photon is due to 5 TeV electron with a magnetic field of 1 mG. Therefore, the calculated flux of non thermal bremsstrahlung from an X-ray result should be modified with the effect of a break of an index.

The energy of a break and an index in a low energy for the knot HST-1 and the knot A are used from Sun et al.(2018). Almost my used data for X-ray spectral analysis corresponds to L state for the knot HST-1(Sun et al. 2018). The modified flux of non thermal bremsstrahlung is shown in table 11.

#### 4.2.2 Comparison with the observed flux with *Fermi*

The fitting parameter of the observed energy spectra with *Fermi* is shown in table 12 and the observed flux with *Fermi* is  $1.7 \times 10^{-9}$  ph/s/cm<sup>2</sup>/GeV at 1 GeV (Abdo et al. 2009). The significance of a spectral form of a broken power law over a power law is 2.7 sigma (Benkhali et al., 2018). Hence, an energy spectra in GeV energy range is still well described with a power law. The flux of non thermal bremsstrahlung of the knot HST-1 of a former data set is close to observed flux with *Fermi*.

For the knot HST-1 of a former data set, flux of non thermal bremsstrahlung with a statistical error is calculated. The upper limit of flux is given by an upper limit of an index in a low energy, an upper limit of an index in a high energy, an upper limit of a flux at 1 keV and a lower limit of an energy of a break. The lower limit of flux is given by a lower limit of an index in a low energy, a lower limit of an index in a high energy, a lower limit of a flux at 1 keV and an upper limit of an energy of a break. The modified flux of non thermal bremsstrahlung from the knot HST-1 is comparable with the observed flux with *Fermi* as shown in table 13. The contribution from the knot HST-1 during a pile up is unknown.

#### 4.2.3 Timescale of flux variability

Flux variability of 2 d is reported in a TeV energy range (Aharonian et al. 2006). The

probability of a detection of flux variability in the GeV energy range is 0.22 with 10 months data (Abdo et al. 2009), 0.018(2.4 sigma) below 10 GeV and 0.23 above 10 GeV with data from 2008 to 2016 (Benkhali et al., 2018). Hence, flux variability has not been detected.

An energy loss time scale of non-thermal bremsstrahlung is given by  $1 / (3.66 \times 10^{-22} N)$  s for a cold material (Longair 1992). Here,  $N$  is a neutral medium density in units of  $\text{m}^{-3}$ . With  $N = 1.0 \times 10^6 \text{ m}^{-3}$  for the knot HST-1, the timescale is  $8.4 \times 10^7$  yr in a jet system,  $1.4 \times 10^7 (6 / \delta)$  yr in an observer system. This long timescale matches with non-flux variability in a GeV energy range and it may indicate a different origin between GeV gamma rays and TeV gamma rays, which is an inverse Compton of synchrotron emission.

The flux of non thermal bremsstrahlung flux is different by a time dependent flux and a time dependent photon index from radio to X-ray band. The non thermal bremsstrahlung from a latter data set of the knot HST-1 is quite below observed flux with *Fermi*. However, non thermal bremsstrahlung from a former data set of the knot HST-1 survive for a long time.

## 5. Conclusion

It is confirmed that an X-ray energy spectra for the nucleus, the knot HST-1 and the knot D are well described with a power law model. It is found that a power law model is rejected statistically for the knot A and an X-ray energy spectra for the knot A is well described with a combination model of a power law and a thermal component. There is a possibility that gas in the jet is heated by a shock and it is observed as a thermal component. Flux of non thermal bremsstrahlung is calculated from an X-ray result with an effect of a break in an index. It is suggested that there is some contribution of non-thermal bremsstrahlung from the knot HST-1 to the observed flux with *Fermi*. The calculated energy spectra in GeV gamma ray is given by  $dN / dE = 5.7 \times 10^{-10} E^{-1.8}$  ph/s/cm<sup>2</sup>/GeV.  $E$  is an energy in units of GeV. An energy loss timescale of non-thermal bremsstrahlung is  $1.4 \times 10^7 (6 / \delta)$  yr. This scenario matches with non-variability in a GeV energy range.

## Acknowledgement

I thank prof. Fukui Y. for NANTEN observation result. I thank prof. Makishima K. and Dr. Matsushita K. for useful comments about data analysis. This research has made use of data obtained from the *Chandra Data Archive*, and software provided by the *Chandra X-ray Center (CXC)* in the application packages *CIAO*.

## Reference

- Abdo A.A. et al., 2009, *ApJ*, 707, 55.
- Abramowski A. et al, 2012, *ApJ*, 746, 151.
- Acciari V.A. et al., 2008, *ApJ*, 679, 397.
- Acciari V.A. et al., 2009. *Sci.*, 325, 444.
- Algaba J.C., Asada K. and Nakamura M., 2016, *ApJ*, 823, 86.
- Aharonian F. et al., 2003, *A&A*, 403, L1.
- Aharonian F. et al. 2006, *Sci.*, 314, 1424.
- Albert J. et al., 2008, *ApJ*, 685, L23.
- Baltz E.A., Briot C., Salati P., Taillet R. and Silk J., 2000, *Phys.ReV.D*, 61, 3514.
- Barkov M.V., Bosch-Ramon V. and Aharonian F., 2012, *ApJ*, 755, 170.
- Belsole E. et al., 2001, *A&A*, 365, L188.
- Benkhali F.A., Chakraborty N. and Rieger F.M, 2018, arXiv1802.03103.
- Biretta J.A., Sparks W.B. and Macchetto F., 1999, *ApJ*, 520, 621.
- Bohringer H. et al., *A&A*, 2001, 365, L181.
- Brinkmann W., Pratt G.W., Rohr S., Kawai N. and Burwitz V., 2007, *A&A*, 463, 611.
- Broderick A.E. and Tchekhovskoy A., 2015, *ApJ*, 809, 97.
- Cui Y-D., Yuan Y-F, Li Y-R. and Wang J-M., 2012, *ApJ*, 746, 177.
- Dainotti M.G., Ostrowski M., Harris D., Siemiginowski A. and Siejkowski H., 2012, *MNRAS*, 426, 218.
- Finke J.D., Dermer C.D. and Bottcher M., 2008, *ApJ*, 686, 181.
- Gebhardt K. & Thomas J., 2009, *ApJ*, 700, 1690.
- Georganopoulos M., Perlman E.S. and Kazanas D., 2005, *ApJ*, 634, L33.
- Giannios D., Uzdensky D.A. and Begelman M.C., 2010, *MNRAS*, 402, 1649.
- Harris D.E., Cheung C.C., Stawarz L., Biretta J.A. and Perlman E.S., 2009, *ApJ*, 699, 305.
- Jong S., Beckman V. Soldi S., Tramacere A. and Gros A., 2015, *MNRAS*, 450, 4333.
- Kalberla P.M.W., Burton W.B., Hartmann D., Arnal E.M., Bajaja E., Morras R. and Poppel W.G.L., *A&A*, 440, 775
- Kino M., Takahara F., Hada K. and Doi A., 2014, *ApJ*, 786, 5.
- Lenain J.P., Boisson C., Sol H. and Katarzynski K., 2008, *A&A*, 478, 111.
- Levinson A. & Rieger F., 2011, *ApJ*, 730, 123.
- Longair M.S., 1992, *High Energy Astrophysics*, second ed. Cambridge.
- Macchetto F. et al., 1997, *ApJ*, 489, 579.
- Marshall H.L., Miller B.P., Davis D.S., Perlman E.S., Wise M., Canizares C.R. and Harris D.E., 2002, *ApJ*, 564, 683.

Meyer E.T. et al., 2013, ApJ, 774, L21.  
Moldowan A., Safi-Harb S., Fuchs Y. and Dubner G., 2005, AdSpR, 35, 1062.  
O'sullivan S.P. et al., 2013, ApJ, 764, 162.  
Perlman E.S. & Wilson A.S., 2005, ApJ, 627, 140.  
Pfrommer C. and Enßlin T.A., 2003, A&A, 407, L73.  
Reimer A., Protheroe R.J. and Donea A.C., 2004, A&A, 419, 89.  
Reynoso M.M., Medina M.C. and Romero G.E., 2011, A&A, 531, A30.  
Rieger F.M. & Aharonian F., 2012, MPLA, 2730030.  
Saxena S., Summa A., Elsasser D., Ruger M. and Mannheim K., 2011, EPJC, 71.1815.  
Seta H., Tashiro M. and Inoue S., 2013, PASJ, 65, 106.  
Stawarz L., Siemiginowska A., Ostrowski M. and Sikora M., 2005, ApJ, 626, 120.  
Stawarz L., Aharonian H., Kataoka J., Ostrowski M., Siemiginowska A. and Sikora M., 2006, MNRAS, 370, 981.  
Stawarz L. et al., 2013, ApJ, 766, 48.  
Sun X-N, Yang R-Z, Riger F.M., Liu R-Y and Aharonian F., 2018, A&A, 612, 106.  
Tavecchio F. & Ghisellini G., 2008, MNRAS, 385, L98.  
Tonry J.L., 1991, ApJ, 373, L1.  
Yamamoto H. et al., 2008, PASJ, 60, 715.  
Wilson A.S. & Yang Y., 2002, ApJ, 568, 133.  
Wong K-W, Nemmen R.S., Irwin J.A. and Lin D., 2017, ApJ, 849, L17.

Table1. The extracted region for each knot of the M87 jet for obsID 1808. 1" is 78 pc.

Name	RA	DEC	Distance from nucleus	radius of Region
large nucleus	12 <sup>h</sup> 30 <sup>m</sup> 49 <sup>s</sup> .40	12°23' 27".9		1".25
nucleus	12 <sup>h</sup> 30 <sup>m</sup> 49 <sup>s</sup> .40	12° 23' 27".9		0".5
HST-1	12 <sup>h</sup> 30 <sup>m</sup> 49 <sup>s</sup> .36	12° 23' 28".3	0".8 (62 pc)	0".6
D	12 <sup>h</sup> 30 <sup>m</sup> 49 <sup>s</sup> .23	12° 23' 28".8	2".8 (218 pc)	0".75
A	12 <sup>h</sup> 30 <sup>m</sup> 48 <sup>s</sup> .60	12° 23' 32".2	12".7 (991 pc)	1".0

Table2.a The observation log used for the large nucleus

obsID	PI	obs date	number
former data set			
1808	Wilson	2000.7	1
11518, 11519, 11520	Harris	2010.4~2010.5	3
13964, 13965	Harris	2011.12~2012.2	2
14973,14974		2012.12~2013.3	2
16042,16043		2013.12~2014.4	2
17056		2014.12	1
exposure time	58.5ks		
latter data set			
17057	Harris	2015.3	1
18809~18813	Cheng	2016.3	5
18232~18233	Russell	2016.2~2016.4	2
18781~18783		2016.2~2016.4	3
18836~18838		2016.4~2016.5	3
18856		2016.6	1
20034~20035	Neilsen	2017.4	2
19457~19458	Wong	2017.2	1
21075~21076		2018.4	1
exposure time	380.4ks		
total exposure time	438.9ks		

Table2.b. The observation log used for the nucleus.

obsID	PI	obs date	number
former data set			
1808	Wilson	2000.7	1
3084, 3087	Harris	2002.2~2002.7	2
3977, 3981	Harris	2002.11~2003.8	2
8579	Birreta	2008.5	1
10282,10284, 10286	Harris	2009.1~2009.12	4
10288			
11516,11520	Harris	2010.4~2010.5	2
16042	Harris	2013.12	1
exposure time	70.0ks		
latter data set			
17057	Harris	2015.3	1
18809,18811,18813	Cheng	2016.3	3
18232,18233	Russell	2016.2~2016.4	2
18781,18782,18783		2016.2~2016.4	3
18837,18838		2016.4~2016.5	2
18856		2016.6	1
19457	Wong	2017.2	1
exposure time	283.5ks		
total exposure time	353.3ks		

Table2.c The observation log used for the knot HST-1

obsID	PI	obs date	number
former data set			
1808	Wilson	2000.7	1
10284,10286,10287	Harris	2009.1~2009.12	4
10288			
11512, 11513, 11516	Harris	2010.4~2010.5	5
11517, 11520			
16042	Harris	2013.12	1
exposure time	59.6ks		
latter data set			
17057	Harris	2015.3	1
18809,18811,18813	Cheng	2016.3	3
18232,18233	Russell	2016.2~2016.4	2
18781,18782,18783		2016.2~2016.4	3
18837,18838		2016.4~2016.5	2
18856		2016.6	1
19457	Wong	2017.2	1
exposure time	283.5ks		
total exposure time	343.1ks		

Table2.d The observation log used for the knot D and the knot A

obsID	PI	obs date	number
former data set			
1808	Wilson	2000.7	1
3084~3088	Harris	2002.2~2002.7	5
3975~3982	Harris	2002.11~2003.8	8
4917~4923	Birreta	2003.11~2004.8	6
(except 4920)			
5737~5748	Birreta	2004.11~2005.5	12
6299~6305	Birreta	2005.11~2006.8	7
7348~7354	Birreta	2006.11~2007.7	7
8510~8517	Harris	2007.2~2007.3	8
8575~8581	Birreta	2008.1~2008.8	7
10282~10288	Harris	2009.1~2009.12	7
11512~11520	Harris	2010.4~2010.5	9
13964~13965	Harris	2011.12~2012.2	2
14973~14974		2012.12~2013.3	2
16042~16043		2013.12~2014.4	2
17056		2014.12	1
exposure time	402.8ks		
latter data set			
17057	Harris	2015.3	1
18809~18813	Cheng	2016.3	5
18232~18233	Russell	2016.2~2016.4	2
18781~18783		2016.2~2016.4	3
18836~18838		2016.4~2016.5	3
18856		2016.6	1
20034~20035	Neilsen	2017.4	2
19457~19458	Wong	2017.2	2
21075~21076		2018.4	2
exposure time	380.4ks		
total exposure time	783.2ks		

Table3 The fitting results with an absorbed power law model for a former data set of each part of a jet. A photo absorption is set free. A photon index  $\alpha$  is defined as  $dN/dE \propto E^{-\alpha}$ . An error is a 90% confidence level statistical error.

	large nucleus	nucleus	HST-1
$N_H(\text{x}10^{20} \text{ cm}^{-2})$	$6.58^{+1.00}_{-0.99}$	$7.82^{+1.28}_{-1.25}$	$4.69^{+1.57}_{-1.54}$
photon index	$2.27^{+0.04}_{-0.04}$	$2.07^{+0.05}_{-0.05}$	$2.40^{+0.07}_{-0.07}$
1keV flux(ph/cm <sup>2</sup> /s/keV)	$8.06^{+0.28}_{-0.26} (\text{x}10^{-4})$	$4.51^{+0.19}_{-0.19} (\text{x}10^{-4})$	$3.60^{+0.20}_{-0.19} (\text{x}10^{-4})$
$\chi^2/\text{d.o.f (d.o.f)}$	0.976(264)	0.954(231)	0.892(172)
	D	A	
$N_H(\text{x}10^{20} \text{ cm}^{-2})$	$1.47^{+0.95}_{-0.94}$	$0.00^{+0.07}$	
photon index	$2.20^{+0.05}_{-0.04}$	$2.39^{+0.01}_{-0.02}$	
1keV flux(ph/cm <sup>2</sup> /s/keV)	$1.17^{+0.04}_{-0.04} (\text{x}10^{-4})$	$3.17^{+0.02}_{-0.02} (\text{x}10^{-4})$	
$\chi^2/\text{d.o.f (d.o.f)}$	0.875(271)	1.218(315)	

Table4 The fitting result with both an absorbed power law model and an absorbed combination model of a power law and an APEC for a former data set of the knot A. A photo absorption is fixed to a 21 cm radio observation value. Here, “PL” is a power law. An error is a 90% confidence level statistical error.

Model		
PL	photon index	$2.46^{+0.01}_{-0.02}$
	1 keV flux(ph/cm <sup>2</sup> /s/keV )	$3.34^{+0.03}_{-0.02} (\text{x}10^{-4})$
	$\chi^2/\text{d.o.f(d.o.f)}$	1.460(316)
PL+APEC	photon index	$2.27^{+0.04}_{-0.03}$
	1keV flux(ph/cm <sup>2</sup> /s/keV )	$2.93^{+0.09}_{-0.10} (\text{x}10^{-4})$
	$kT(\text{keV})$	$0.23^{+0.02}_{-0.03}$
	abundance	$0.00^{+0.02}$
	normalization	$2.07^{+0.64}_{-0.65} (\text{x}10^{-3})$
	$\chi^2/\text{d.o.f (d.o.f)}$	1.030(313)

Table 5 The fitting result with an absorbed power law model for a latter data set of each part of a jet. A photo absorption is set free. An error is a 90% confidence level statistical error.

	large nucleus	nucleus	HST-1
$N_{\text{H}}(\text{x}10^{20} \text{ cm}^{-2})$	$6.94^{+0.76}_{-0.74}$	$11.2^{+1.40}_{-1.40}$	$2.40^{+1.86}_{-1.80}$
photon index	$2.22^{+0.02}_{-0.02}$	$2.22^{+0.04}_{-0.04}$	$2.27^{+0.06}_{-0.06}$
1keV flux(ph/cm <sup>2</sup> /s/keV)	$5.19^{+0.11}_{-0.10} (\text{x}10^{-4})$	$2.75^{+0.10}_{-0.11} (\text{x}10^{-4})$	$1.21^{+0.07}_{-0.06} (\text{x}10^{-4})$
$\chi^2/\text{d.o.f (d.o.f)}$	1.498(397)	1.240(297)	0.916(218)
	D	A	
$N_{\text{H}}(\text{x}10^{20} \text{ cm}^{-2})$	$3.64^{+1.36}_{-1.34}$	0.00	
photon index	$2.30^{+0.05}_{-0.04}$	$2.32^{+0.03}_{-0.02}$	
1keV flux(ph/cm <sup>2</sup> /s/keV)	$1.63^{+0.06}_{-0.07} (\text{x}10^{-4})$	$2.57^{+0.03}_{-0.04} (\text{x}10^{-4})$	
$\chi^2/\text{d.o.f (d.o.f)}$	0.930(273)	1.137(296)	

Table 6 The fitting result with an absorbed power law model for a latter data set of the knot A. A photo absorption is fixed to a 21 cm radio observation value. An error is a 90% confidence level statistical error.

photon index	$2.37^{+0.02}_{-0.02}$
1 keV flux(ph/cm <sup>2</sup> /s/keV)	$2.68^{+0.04}_{-0.04} (\text{x}10^{-4})$
$\chi^2/\text{d.o.f (d.o.f)}$	1.203(297)

Table 7 The fitting result with an absorbed power law model for all data of each part of a jet. A photo absorption is set free. An error is a 90% confidence level statistical error.

	large nucleus	nucleus	HST-1
$N_{\text{H}}(\text{x}10^{20} \text{ cm}^{-2})$	$4.61^{+0.57}_{-0.56}$	$6.33^{+0.90}_{-0.88}$	$0.00^{+0.35}$
photon index	$2.21^{+0.02}_{-0.02}$	$2.15^{+0.03}_{-0.03}$	$2.37^{+0.02}_{-0.03}$
1keV flux(ph/cm <sup>2</sup> /s/keV)	$5.48^{+0.10}_{-0.09} (\text{x}10^{-4})$	$3.03^{+0.09}_{-0.08} (\text{x}10^{-4})$	$1.71^{+0.02}_{-0.02} (\text{x}10^{-4})$
$\chi^2/\text{d.o.f (d.o.f)}$	1.496(410)	1.247(334)	0.929(257)
	D	A	
$N_{\text{H}}(\text{x}10^{20} \text{ cm}^{-2})$	$3.46^{+0.74}_{-0.74}$	0.00	
photon index	$2.24^{+0.03}_{-0.03}$	$2.40^{+0.01}_{-0.02}$	
1keV flux(ph/cm <sup>2</sup> /s/keV)	$1.37^{+0.04}_{-0.03} (\text{x}10^{-4})$	$2.99^{+0.01}_{-0.02} (\text{x}10^{-4})$	
$\chi^2/\text{d.o.f (d.o.f)}$	0.973(333)	1.515(370)	

Table 8 The fitting result with an absorbed power law model for all data of the knot HST-1, an absorbed power law model (top) and an absorbed combination model of power law and APEC (middle, bottom) for all data of the knot A. A photo absorption is fixed to a 21 cm radio value. The temperature is two types. One is set free and the other is set as 0.2 keV. An error is a 90% confidence level statistical error.

Model		HST-1	A
PL	photon index	$2.42^{+0.02}_{-0.03}$	$2.46^{+0.02}_{-0.01}$
	1keV flux(ph/cm <sup>2</sup> /s/keV)	$1.79^{+0.03}_{-0.02} (\text{x}10^{-4})$	$3.14^{+0.02}_{-0.01} (\text{x}10^{-4})$
	$\chi^2/\text{d.o.f (d.o.f)}$	0.988(258)	1.869(371)
PL+APEC	photon index		$2.97^{+0.09}_{-0.09}$
	1 keV flux(ph/cm <sup>2</sup> /s/keV)		$2.30^{+0.13}_{-0.18} (\text{x}10^{-4})$
	$kT(\text{keV})$		$7.41^{+1.02}_{-0.68}$
	abundance		$0.00^{+0.03}$
	normalization		$3.18^{+0.59}_{-0.21} (\text{x}10^{-4})$
	$\chi^2/\text{d.o.f (d.o.f)}$		1.193(368)
PL+APEC( $kT=0.2$ keV)	photon index		$2.30^{+0.02}_{-0.02}$
	1keV flux(ph/cm <sup>2</sup> /s/keV)		$2.80^{+0.04}_{-0.05} (\text{x}10^{-4})$
	abundance		$0.00^{+0.01}$
	normalization		$2.46^{+0.51}_{-0.78} (\text{x}10^{-3})$
	$\chi^2/\text{d.o.f (d.o.f)}$		1.162(369)

Table 9 Physical values for a former data set, a latter data set and all data. Here, “PL” is a power law.

name	Best Model	Neutral density $N$ ( $\text{cm}^{-3}$ )	plasma density $n_i$ ( $\text{cm}^{-3}$ )	$p=2\alpha-1$	$K'(\text{m}^{-3}\text{GeV}^{p-1})$
former data set					
large nucleus	PL	0.8		3.5	$2.3 \times 10^{-7}$
nucleus	PL	2.6		3.1	$4.0 \times 10^{-7}$
HST-1	PL	1.0		3.8	$5.9 \times 10$
D	PL	0.0		3.4	$4.3 \times 10^{-1}$
A	PL+APEC	>0.0	10.5	3.5	$8.7 \times 10^{-1}$
latter data set					
nucleus	PL	4.0		3.4	$7.9 \times 10^{-7}$
HST-1	PL	0.3		3.5	1.5
D	PL	0.6		3.6	3.0
A	PL	0.0		3.7	10.7
all data					
nucleus	PL	2.0		3.3	$8.7 \times 10^{-7}$
HST-1	PL	0.0		3.8	$2.9 \times 10$
D	PL	0.5		3.5	2.5
A	PL+APEC( $kT=0.2$ keV)	>0.0	11.4	3.6	2.2

Table 10 The calculated flux of non thermal bremsstrahlung at 1 GeV from an X-ray result for a former data set, a latter data set and all data.

Name	$N+n_i$ (cm <sup>-3</sup> )	$p$	$K'$ (m <sup>-3</sup> GeV <sup>p-1</sup> )	flux at 1 GeV with $p$ (ph/s/cm <sup>2</sup> /GeV)
former data set				
large nucleus	0.8	3.5	$2.3 \times 10^{-7}$	$3.6 \times 10^{-14}$
nucleus	2.6	3.1	$4.0 \times 10^{-7}$	$3.1 \times 10^{-17}$
HST-1	1.0	3.8	$5.9 \times 10$	$1.5 \times 10^{-4}$
D	0.0	3.4	$4.3 \times 10^{-1}$	0.0
A	10.5	3.5	$8.7 \times 10^{-1}$	$9.7 \times 10^{-7}$
latter data set				
nucleus	4.0	3.4	$7.9 \times 10^{-7}$	$8.9 \times 10^{-21}$
HST-1	0.3	3.5	1.5	$1.1 \times 10^{-8}$
D	0.6	3.6	3.0	$3.7 \times 10^{-13}$
A	0.0	3.7	10.7	0.0
all data				
nucleus	2.0	3.3	$8.7 \times 10^{-7}$	$1.1 \times 10^{-21}$
HST-1	0.0	3.8	$2.9 \times 10$	0.0
D	0.5	3.5	2.5	$5.6 \times 10^{-14}$
A	11.4	3.6	2.2	$1.2 \times 10^{-11}$

Table 11 The modified flux of non thermal bremsstrahlung at 1 GeV with an effect of a break in an index for the knot HST-1 and the knot A. An index in a lower band  $\alpha_1$  and an energy of a break  $E_{\text{break}}$  are used from Sun et al.(2018). The error is 68% confidence level statistical error.

	$\alpha_1$	$E_{\text{break}}$ (GeV)	modified flux(ph/s/cm <sup>2</sup> /GeV) at 1 GeV
HST-1(former)	$1.77 \pm 0.07$	$460^{+20}_{-30}$	$5.7 \times 10^{-10}$
HST-1(latter)	$1.77 \pm 0.07$	$460^{+20}_{-30}$	$3.5 \times 10^{-13}$
A(former)	$2.30^{+0.04}_{-0.03}$	$480 \pm 20$	$1.0 \times 10^{-12}$

Table 12 The fitting parameters of the observed flux with *Fermi* with a power law of  $dN/dE=(a(E/\text{GeV})^{-b+c})$ .

	value	MIGRAD error
a(ph/s/cm <sup>2</sup> /GeV)	$1.7 \times 10^{-9}$	$0.2 \times 10^{-9}$
b	2.39	0.15
c(ph/s/cm <sup>2</sup> /GeV)	$2.0 \times 10^{-12}$	$3.4 \times 10^{-12}$

Table 13 The comparison between modified flux of non thermal bremsstrahlung and the observed flux with *Fermi*. The lower limit and upper limit of flux by a statistical error are shown.

	(ph/s/cm <sup>2</sup> /GeV)	lower (ph/s/cm <sup>2</sup> /GeV)	upper (ph/s/cm <sup>2</sup> /GeV)
<i>Chandra</i> (HST-1 former)	$5.7 \times 10^{-10}$	$8.3 \times 10^{-11}$	$1.7 \times 10^{-8}$
<i>Fermi</i>	$1.7 \times 10^{-9}$	$1.5 \times 10^{-9}$	$1.9 \times 10^{-9}$

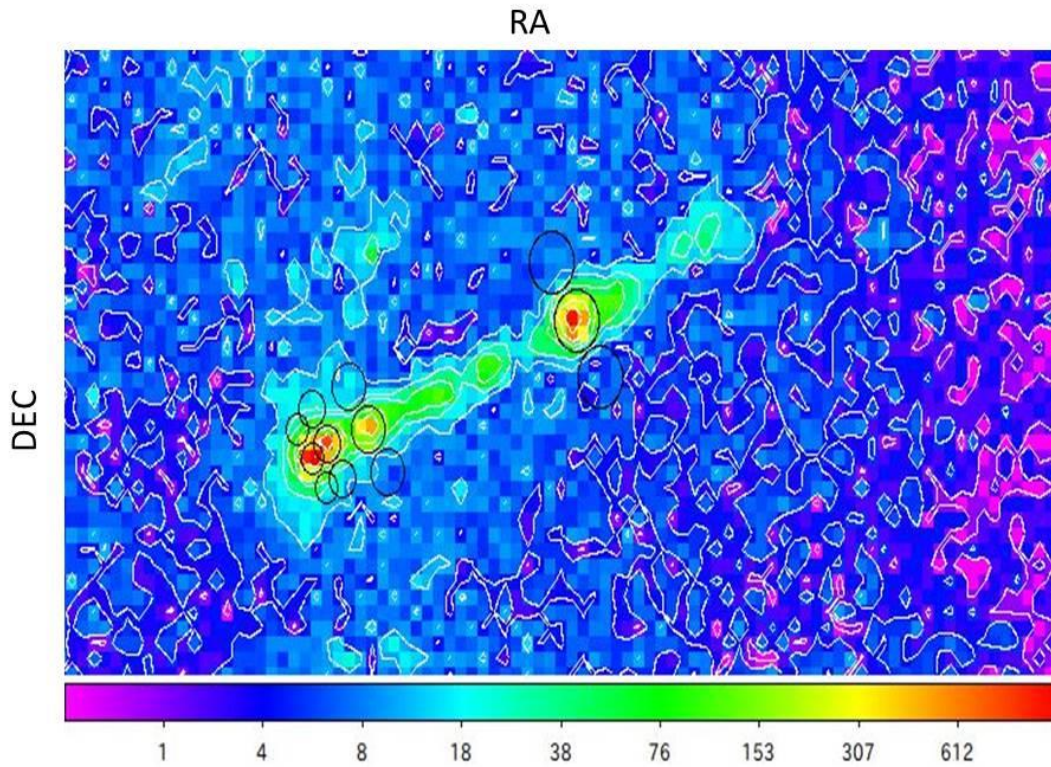


Figure1. An X-ray image of the M87 jet for obsID 1808 with *Chandra*. From left, the nucleus, the knot HST-1, the knot D, the knot A, and each background region, respectively.

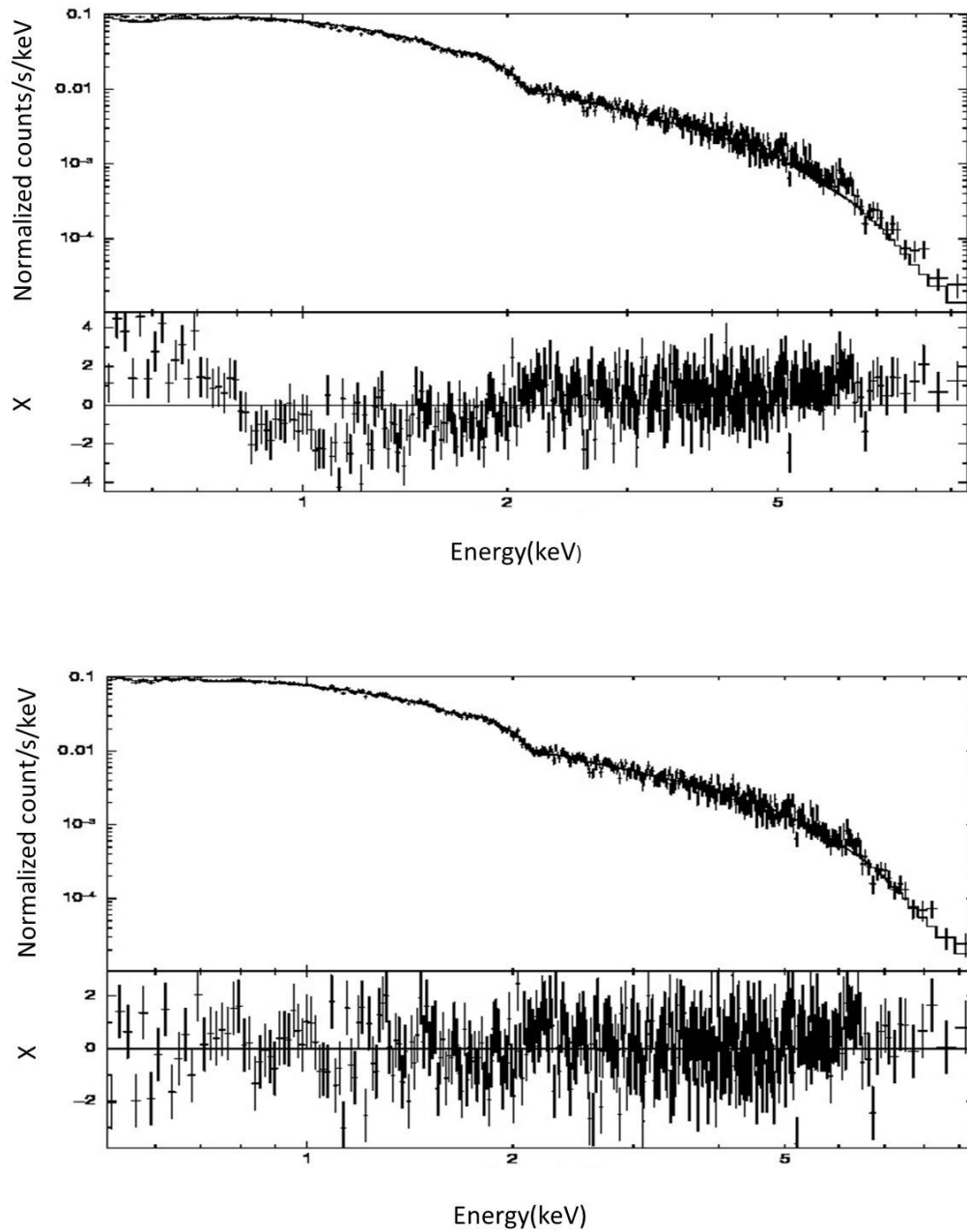


Figure2. The fitted X-ray energy spectra with two kinds of model for all data of the knot A. The models are an absorbed power law(top) and an absorbed combination of a power law and an APEC (bottom). A photo absorption is fixed to a 21 cm radio observation value.

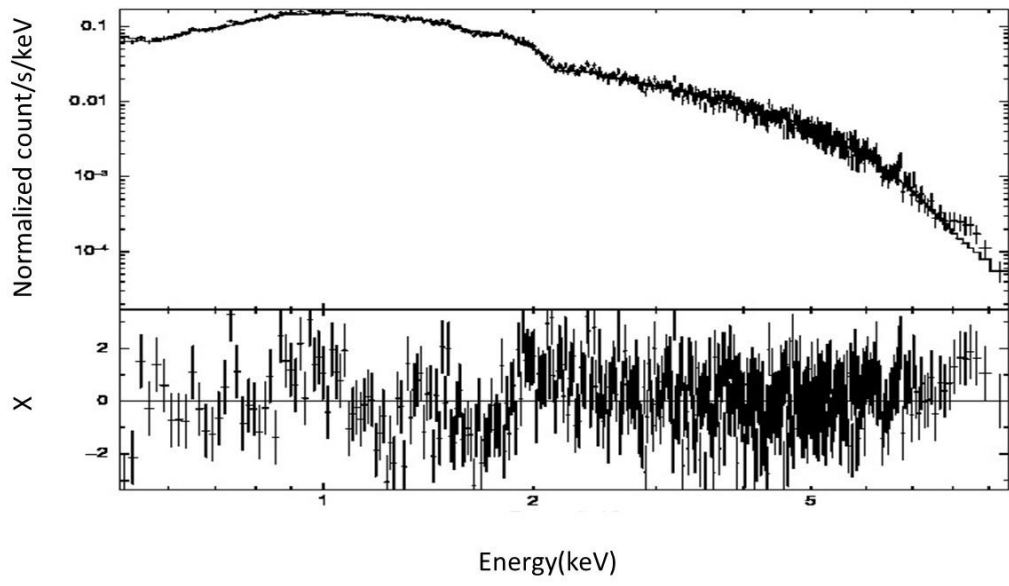


Figure3. The fitted X-ray energy spectra with an absorbed power law for all data of the large nucleus.